ARC Geophysical Research

Phloem Catastrophe: Using Bifurcation Analysis to Predict Plant Tipping Points

Louis Youssef[1], Mazen Nakad[*2], Jean-Christophe Domec[3], Sanna Sevanto[4], and Gabriel Katul[5]

[1]Department of Plant Science, McGill University, Montreal, Canada
[2]Chemical Engineering Program, School of Engineering, Lebanese American University, Byblos, Lebanon
[3]Bordeaux Sciences Agro, UMR 1391 INRA-ISPA, France
[4]Earth and Environmental Sciences Division, Los Alamos National Laboratory, Los Alamos, NM, USA
[5]Department of Civil and Environmental Engineering, Duke University, Durham, NC, USA

Abstract

A mathematical framework is developed to analyze phloem failure in plants using bifurcation analysis and catastrophe theory. The framework balances sucrose production from leaf photosynthesis modeled using stomatal optimality theory with sucrose transport through the much studied pressure-driven Münch mechanism. The model also integrates xylem water potential, osmotic gradients, and sucrose sink strength along the phloem. Systematic variation of key control variables, including xylem water potential and sucrose removal rate, reveals the emergence of multiple equilibria and identifies thresholds beyond which phloem transport becomes dynamically unstable to small perturbations. Phloem failure is shown to arise through a saddle-node bifurcation, characterized by two stable sucrose loading concentration states separated by an unstable intermediate one. The lower concentration stable state is within the range of sucrose loading values reported in the literature. Such phloem catastrophe was mathematically analogous to critical transitions in other eco-hydrological systems including xylem cavitation in plants. The analysis provides a mechanistic basis for quantifying phloem vulnerability and indicates that vascular stability requires coordination and balance between photosynthetic supply of sucrose and phloem hydraulic capacity.

Keywords: Bifurcation Analysis, Catastrophe Theory, Münch Mechanism, Plant Hydraulics, Sucrose Transport, Stomatal Optimality Theory, Tipping Points

*Corresponding Author
E-mail address: mazen.nakad@gmail.com
doi:10.5149/ARC-GR.2526

1 Introduction

Sucrose transport in the phloem is of significance because it is the main mechanism by which plants distribute the products of photosynthesis for growth, storage, development, and stress responses across the entire organism [11, 46, 48, 99, 109]. The pressure-flow hypothesis (PFH), first formulated by E. Münch in the early 1930s in his book titled "Movement of Substances in Plants", provides the foundations for a mathematical model describing long-distance sugar transport in the phloem [66]. The PFH replaced prior theories that proposed that protoplasmic streaming carries solutes cell to cell or that active transport occurred along each sieve element [93]. Support for the PFH was provided from radioactive labeling studies in crops and short canopy plants [4, 5, 11, 27]. These studies demonstrated that the magnitude and downward direction of metabolite movement appeared to be fast (∼100 cm/h), almost 10 times faster than xylem water transport [78], and related to concentration differences at source and sink and inversely related to the distance between them (i.e. a gradient from source to sink). The radioactive labeling velocity estimates were also in close agreement with earlier (in 1922) and independent calculations that found phloem transport to be fast (∼50 cm/h) and non-diffusive [20]. Similar estimates reported by others using different assumptions or tracers arrived at velocities ranging from 16-160 cm/h in short crops [4, 16, 106]. These speeds cannot be reconciled with cell to cell transport along each sieve element lending support to the PFH [26]. With such initial experimental support, the significance of PFH to plant hydraulics now parallels that of the cohesion-tension theory (CTT) describing water transport in the xylem [2, 21, 38, 45, 103, 105]. However, direct experimental access to phloem transport remains limited to short plants and short experimental periods [62, 104], which necessitates the continued reliance on mathematical models to probe hypotheses about phloem function and - no less important - dysfunction [30, 35, 64].

According to the PFH, the gradient in sucrose concentration between the loading area (near the leaves) and unloading area (near the roots) generates positive turgor pressure gradient that drives water flow. Because water is incompressible, inflow of water occurs from the xylem near the top and the outflow occurs near the bottom [97, 104]. While widely accepted, several challenges persist for tall plants, where the increase in hydraulic resistance is presumed to require larger loading concentrations [25, 43, 47, 83]. In addition, several aspects such as phloem elasticity, the hydraulic resistance of sieve plates, and sucrose unloading dynamics are still being worked out [69, 88, 90, 101], which further complicates theoretical models. Beyond these local phloem dynamics, sucrose transport is also influenced by the surrounding organs. Leaf stomata function as the primary conduits of carbon dioxide from the atmosphere into the plant, where photosynthesis converts these carbon dioxide molecules into sugars and oxygen molecules [13, 17, 23, 29, 41, 61]. These sugars are loaded into the phloem (passively or actively) and act as a sucrose source in the phloem. This source activity is further constrained by a feedback from assimilate transport and the balance between supply and demand across the plant [71, 89]. Once exported, sucrose is transported along the stem, which serves as a metabolic sink supporting cambial growth and repair [33, 60]. Roots contribute an additional sink for sucrose, including root-exudation [8, 89, 100] while simultaneously influencing the hydraulic status of the canopy through their role in soil water uptake [14, 53]. Taken together, this whole-plant perspective emphasizes that sucrose transport in the phloem cannot be 'divorced' from the 'bottlenecks' in the carbon entry and the hydraulic constraints provided by the soil–xylem system [24, 32, 71].

Water transport in the xylem also plays a role in regulating phloem function [28, 48, 111].

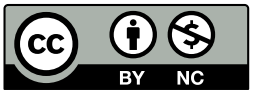

Radial exchange between the two tissues facilitates the maintenance of the pressure balance and the movement of water along the pathway, with xylem water potential acting as a reference potential that governs water exchange [45, 98]. Under high transpiration or drought stress, declines in xylem water potential restrict water entry into the phloem, which reduces its transport capacity [86]. Nevertheless, water exchange between the xylem and the phloem can buffer short-term fluctuations in xylem water storage, allowing transient adjustment to environmental variations [87, 91]. These findings show the importance of analyzing PFH beyond a purely osmotic framework to one embedded within whole-plant hydraulics and stress physiology [38, 45, 48, 74]. Yet, structural and functional mechanisms that interactively initiate phloem dysfunction that ultimately lead to phloem failure remain less understood despite their role in transport and plant survival under stress [79].

To address this knowledge gap, a framework based on bifurcation analysis, tipping points, and catastrophe theory is proposed to investigate phloem failure in the most generic terms. Bifurcation analysis provides a mathematical framework for a qualitative understanding of how gradual changes in key control variables can induce sudden and irreversible shifts in system behavior [81, 92]. Initiated by H. Poincaré in the late 1800s [76] and later formalized by A. Lyapunov, E. Hopf, and R. Thom [94–96], these theories have been widely applied in ecology to describe tipping points in population dynamics, food web stability, and ecosystem collapse [34, 40, 45, 51, 52, 57, 59, 63, 84, 85, 94, 112]. Abrupt transitions, referred to as catastrophes, occur when a gradual change in a control variable drives a nonlinear system to a critical threshold where the nature of the equilibrium changes, for example when a stable equilibrium becomes unstable through a fold bifurcation. In this case, the system can no longer maintain stability and rapidly switch to another equilibrium state or collapses altogether.

Here, bifurcation analysis is applied to sucrose transport dynamics governed by the PFH to identify conditions that preserves stable phloem transport versus those that precipitate phloem collapse. The framework links leaf photosynthesis, modeled through stomatal optimality theory [42, 56, 65, 70], with phloem hydrodynamics [31, 67], thereby enabling a systematic exploration of phloem catastrophes. The analysis focuses on the relation between state variables such as sucrose loading concentration and functional or structural control variables including xylem water potential, sucrose unloading rate from photosynthesis, phloem radius, and hydraulic path length assumed to be proportional to plant height. Under normal conditions, the phloem maintains steady carbohydrate flow from leaves to sinks, but perturbations such as drought (lowering xylem water potential) or increased sucrose removal (e.g. herbivory) can push the phloem system beyond a tipping point into irreversible failure. By treating these drivers as control variables that can be dialed up or down, bifurcation analysis in conjunction with the Münch mechanism is proposed here to map the critical thresholds that separate stable operation from collapse.

2 Theory

The mathematical framework for analyzing phloem failure in plants assumes that, at equilibrium, the overall sucrose production from leaf photosynthesis is primarily balanced by the transport capacity of the phloem vasculature. This balance is expressed in terms of the sucrose loading concentration at the source c_0. The sucrose production rate PR depends on photosynthetic assimilation derived from stomatal optimality. The transport rate TR is governed by the PFH, where osmotic gradients draw water from the xylem into the phloem and drive bulk flow opposed by viscous resistance.

In what follows, the photosynthetic formulation that defines PR and its dependence on stomatal optimality is first presented. The phloem transport equations that govern TR under the pressure-flow hypothesis are then described. Bifurcation analysis is presented in which

the equilibrium condition $PR = TR$ is coupled with stability analysis to identify the sucrose loading concentrations at equilibrium c_0^* and to classify their stability under slowly varying environmental and structural control variables. The need for coordinating between photosynthetic properties and phloem structural properties is then discussed.

Symbol	Description	Value (Unit)
c	sucrose concentration	- (mol/m^3)
c_a	atmospheric carbon dioxide concentration	400 (ppm)
c_b	concentration in surrounding sink cells	10 (mol/m^3)
c_o	sucrose loading concentration	- (mol/m^3)
g	leaf stomatal conductance	- (mol m^{-2} s^{-1})
k	membrane permeability	10^{-14}(m Pa^{-1} s^{-1})
p	phloem turgor pressure	- (Pa)
p_m	leaf water tension	- (Pa)
r	phloem tube radius	- (m)
t_r	removal time	- (s)
u	sap flow axial velocity	- (m/s)
x	location along phloem tube	- (m)
A	photosynthetic rate per leaf area	- (mol m^{-2} s^{-1})
$C_{o,a}$	O_2 in atmosphere	210 (mmol/mol)
D	molecular diffusivity of sucrose in water	4×10^{-10} (m^2/s)
H	Hamiltonian for deriving optimal g	- (mol m^{-2} s^{-1})
I	photosynthetically active radiation	800 (µmol m^{-2} s^{-1})
J	Sucrose mass flux	- (mol m^{-2} s^{-2})
$J_{c,\max}$	max rate of electron transport	2.1 $V_{c,max}$ (µmol m^{-2} s^{-1})
$K_{c,o}$	Michaelis constant for CO_2 fixation	300 (µmol/mol)
$K_{o,a}$	Michaelis constant for O_2 inhibition	300 (mmol/mol)
L	plant height	- (m)
L_a	total leaf area	32.5 (m^2)
L_{th}	max transport length	- (m)
P_a	total phloem cross-sectional area	8.25×10^{-4} (m^2)
R_g	ideal gas universal constant	8.314 (J mol^{-1} K^{-1})
T	temperature	298 (K)
$V_{c,\max}$	max carboxylation capacity	59 (µmol m^{-2} s^{-1})
VPD	vapor pressure deficit	1.9 (kPa)
α	interaction strength between c_0 and A	1200 (mol/m^3)
α_p	apparent quantum yield coeff.	0.064 (mol/mol)
β_1	photosynthetic parameter	- (µmol m^2 s^{-1})
β_2	photosynthetic parameter	- (µmol/mol)
β_3	long-term c_i/c_a	- (dimensionless)
δ	interaction strength between c_0 and A	1600 (mol/m^3)
λ	Lagrange multiplier / marginal water use efficiency	- (µmol mol^{-1} kPa^{-1})
Ψ_{water}	water potential difference driving radial flow	- (Pa)
ρ	sap density	1000 (kg/m^3)
μ	dynamic viscosity	- (Pa s)

Table 1: Description of the main symbols, their units, and numerical values when held constant in the bifurcation analysis. The symbol '-' indicates quantities that are either calculated or varied in the sensitivity analysis.

2.1 Sucrose Production Rate (PR)

Sucrose production is initiated by leaf photosynthesis, where it establishes the osmotic potential gradient required for translocation from leaves to sink organs. To represent this process, different formulations for leaf stomatal conductance and photosynthesis can be employed, ranging from empirical models [13, 49] to those grounded in optimality theory [15, 29, 41, 42]. Stomatal optimality theory is adopted here as it provides a mechanistic link between leaf carbon assimilation, leaf stomatal conductance and overall water availability in the rooting zone. Environmental conditions set a maximum photosynthesis rate per unit leaf area that then gets reduced once a feedback to increasing sucrose concentration is initiated at high c_0. Once the rate of CO_2 uptake from the atmosphere is determined at the leaf scale, a carbon balance equation is required to allocate carbon supply to various sinks including phloem loading. For simplicity, it is assumed that a constant fraction of assimilated carbon molecules are converted to sucrose and then loaded into the phloem.

Stomatal optimality theory combines the Farquhar photosynthesis model for biochemical demand [23] with the diffusional transport of carbon dioxide from the atmosphere into the mesophyll under the assumption that stomatal conductance g adjusts to maximize carbon gain for a given water availability in the rooting zone per unit leaf area [44, 56]. Solutions to this framework have been derived for both static [29, 42, 61] and dynamic [56, 65] marginal water use efficiencies. The main assumption of optimality theory is that plants regulate stomatal conductance to maximize carbon gain per leaf area A constrained by a root-zone soil water availability per leaf area [15]. The optimization can thus be formulated for a quasi-static case when the marginal water-use efficiency λ is slowly evolving compared to the time scale of stomatal opening and closure. For the dynamic case, λ must co-evolve with root-zone soil water availability and g. In both cases, stomata are assumed to adjust g such that the Hamiltonian H is maximized, leading to the condition

$$\frac{\partial H}{\partial g} = \frac{\partial A}{\partial g} - \lambda \frac{\partial E}{\partial g}, \tag{1}$$

where E is transpiration per unit leaf area. To evaluate this condition, A and E must be expressed as functions of g. Transpiration is generally driven by the water vapor concentration gradient, approximated by the vapor pressure deficit VPD when leaves are well coupled to the atmosphere (i.e very large aerodynamic conductance compared to g). The A is obtained by equating atmospheric supply of carbon dioxide through Fickian diffusion with photosynthetic demand described by the Farquhar biochemical demand for C_3 plants [23] resulting in

$$A = g(c_a - c_i) = \beta_1 \frac{(c_i - c_p)}{\beta_2 + c_i}, \tag{2}$$

$$E = 1.6\, g\, \mathrm{VPD}, \tag{3}$$

where c_a and c_i are the ambient and intercellular CO_2 concentrations, c_p is the CO_2 compensation point, and β_1, β_2 are photosynthetic parameters determined by either RuBP regeneration or RuBisCO activity limitation, respectively. These formulations allow g to be linked to environmental drivers (e.g. air temperature, c_a, VPD, and photosynthetically active radiation) with the effects of soil water status embedded in λ (explicitly in the case of dynamic optimization and implicitly in the case of static optimization). The full (and lengthy) formulation of the static solution (i.e. slowly varying λ relative to opening and closure of stomatal aperture), which is employed here, is detailed elsewhere [42]. A simplified version, which retains the same parameter structure as the nonlinear model, is featured for illustration and is provided in Appendix A.

Several expressions for λ have been proposed [56]. Here, λ is assumed to increase linearly with leaf water tension p_m (defined later as the maximum background pressure, representing the peak spatial tension along the phloem pathway), reflecting reduced water availability in the rooting zone. It is expressed as

$$\lambda = \lambda_{\min} + \frac{p_m}{3}\left(\lambda_{\max} - \lambda_{\min}\right), \tag{4}$$

where $\lambda_{\max}$ and $\lambda_{\min}$ correspond to complete stomatal closure and maximum opening, respectively. More complex formulations, including those based on dynamic optimality theories [65], could also be adopted. Additional non-stomatal controls on photosynthesis, such as mesophyll conductance, are not explicitly treated here since they predictably affect A in ways that do not qualitatively alter the bifurcation analysis [19, 58, 77, 80, 107].

As discussed earlier, the assimilated carbon is directly loaded into the phloem at steady state. The production rate depends on A determined from the optimality theory. This rate is then up-scaled to the whole-plant level using the total plant leaf area L_a. The L_a is determined by the product of the number of leaves per tree and the representative surface area of leaves. Once the total photosynthetic rate is determined, a down-regulation function with increasing c_0 is introduced on A to reflect the negative feedback due to large sucrose (or carbon) concentration within the leaf [1]. A model of maximum simplicity reflecting this feedback on A and PR is [71],

$$PR = L_a \times A_{eff};\ A_{eff} = A \times \begin{cases} 1, & c_0 < 1200\ \text{mol/m}^3 \\ 1 - (c_0 - \alpha)/\delta, & 1200 \le c_0 < 2800\ \text{mol/m}^3 \\ 0, & c_0 \ge 2800\ \text{mol/m}^3, \end{cases} \tag{5}$$

where A is determined from optimality theory (using Equation 13 in Appendix A), coefficients α and δ describe the strength of the interaction between c_0 and A (where c_0 is expressed per unit phloem sap volume). This down-regulation function provides an ad-hoc representation of an instantaneous feedback that decreases leaf carbon assimilation when high ($c_0 > 1200$ mol/m^3). In this formulation, the effective leaf assimilation rate is A_{eff} that is converted to PR=$A_{eff}L_a$ assuming all assimilated carbon is loaded into the phloem. In reality, part of the assimilated carbon is respired or temporarily stored as starch [1, 71], which would trigger earlier stomatal closure as leaves respond to accumulated assimilates prior to phloem export. This lag is ignored in the equilibrium and bifurcation analysis to be conducted.

2.2 Sucrose Transport Capacity (TR)

Sucrose loading at the source and unloading at the sink establish osmotic gradients that draw water from the xylem to generate the pressure difference necessary to drive the bulk flow phloem sap [104]. The sap is modeled as an incompressible Newtonian fluid with constant density ρ (assumed equal to the density of water) and spatially constant dynamic viscosity μ. Concentration-dependent viscosity can influence local flow dynamics, particularly under large sucrose gradients between source and sink [68]. However, the limiting case for phloem failure is when μ is uniformly at its highest value. While local viscosity gradients are not resolved in this study, a uniform viscosity dependence on concentration is incorporated as discussed later. This approximation is used for simplicity and provides a reasonable representation when sucrose concentration varies gradually along the phloem. The flow is assumed to operate at very low Reynolds number (i.e. creeping flow) such that viscous forces dominate over inertia [38]. Under these conditions, inertial terms in the momentum balance can be neglected and the mean axial velocity is directly related to the local pressure gradient through the

Hagen–Poiseuille relation [30, 36, 97]. Frictional resistance from sieve plates is also neglected here, although it may contribute additional energy dissipation above and beyond wall viscous stresses [43, 88].

The derivation of the governing equations for the flow field has been provided elsewhere [36, 67, 97], and only the main relations with the added control variables for the bifurcation analysis are presented. Conservation of water mass applied to a control volume formed by an infinitesimal phloem segment of radius r and length Δx surrounded by a xylem reservoir is expressed as [36]

$$\pi r^2 \Delta u + 2\pi r \ \Delta x \ k \ \Psi_{water} = 0, \tag{6}$$

where $\Delta u = (\Delta x)(\partial u/\partial x)$ (i.e. expanded using a first-order Taylor series), u is the axial velocity, k is the hydraulic permeability of the phloem–xylem interface assumed to be constant along the conduit, and Ψ_{water} is the local water potential difference driving radial exchange (i.e. gravitational potential differences between xylem and phloem at position x cancels). The water potential difference is then expressed as the sum of xylem tension, phloem turgor, and osmotic potential,

$$\Psi_{water} = \underbrace{-p_m \left(1 - \frac{x}{L}\right)}_{xylem\ pressure} - \underbrace{p(x)}_{phloem\ turgor} + \underbrace{R_g \ T \ c(x)}_{osmotic\ pressure}, \tag{7}$$

where the first term corresponds to the xylem water pressure, idealized as a linear decline from 0 MPa at the root positioned at $x = L$ (phloem length) to a maximum leaf water tension p_m at the leaf level set at $x = 0$; the second term represents the phloem turgor pressure p; and the third term corresponds to the osmotic potential in the phloem, approximated here by the van't Hoff relation with R_g being the universal gas constant, T the sap temperature, and c the sucrose concentration. In reality, the xylem water potential profile is not linear and depends on the xylem hydraulics [40] as water moves from the roots to the leaves. A linear profile is nevertheless assumed here as a tractable approximation for the bifurcation analysis since it allows water stress to be parameterized in terms of a single leaf water tension p_m. Other non-linear shapes arising from soil-plant xylem hydraulics can be used [54] but at the expense of introducing additional control variables for representing these plant hydraulics.

By taking $\Delta x \to 0$ and replacing Ψ_{water} in Equation 6, a relation between c, u and p is obtained, and Equation 6 becomes

$$\frac{r}{2}\frac{\partial u}{\partial x} = k \left[R_g T c(x) - p(x) - p_m \left(1 - \frac{x}{L}\right)\right]. \tag{8}$$

It indicates that axial flow in the phloem is sustained by the radial inflow and outflow of water exchanged with the xylem to conserve water mass within the phloem. Near the source, high sucrose loading lowers the phloem water potential below that of the xylem, drawing water inward and pushing the sap axially. Toward the sink, the opposite occurs: as sucrose concentration decreases, the phloem water potential rises above that of the xylem, allowing water to move back into the xylem or toward the roots. The resulting sap flow along the phloem establishes a pressure gradient that develops in opposition to viscous resistance.

Because the flow occurs at low Reynolds number and under the slender-tube approximation $r/L \ll 1$, the radial momentum balance can be neglected. Under this assumption, the axial momentum balance is reduced to the Hagen–Poiseuille relation

$$u = -\frac{r^2}{8\mu}\frac{\partial p}{\partial x}. \tag{9}$$

Unlike the classical Hagen–Poiseuille flow induced by a uniform pressure gradient, the driving gradient in the phloem is spatially variable and depends on local sucrose concentration through

osmotic effects [9, 75, 110]. The μ is treated as spatially constant along the conduit but parameterized as a function of the loading concentration c_0 using an empirical neural-network correlation [6]. This representation will be a limiting scenario in the bifurcation analysis because phloem transport is limited by the highest viscosity along its path as noted earlier. However, this formulation accommodates the fact that higher loading concentrations increase effective viscosity, which lowers transport capacity by enhancing viscous dissipation, consistent with theoretical predictions and experimental evidence [37].

When the water balance in Equation 8 is combined with the Hagen–Poiseuille approximation in Equation 9, the axial velocity u is eliminated and an expression for the pressure of the phloem p is obtained,

$$\frac{r^3}{16\mu k}\frac{\partial^2 p}{\partial x^2} - p = -R_g\ T\ c(x) + p_m\left(1 - \frac{x}{L}\right). \tag{10}$$

This equation emphasizes the role of the background xylem pressure in regulating phloem transport. Under water-limited conditions, represented here by an increase in leaf water tension p_m, higher sucrose concentrations are required at the loading site to offset xylem tension, draw water into the phloem, and maintain positive turgor. Because phloem tissue is composed of living cells with substantially reduced cell wall lignification compared to xylem conduits, maintaining positive pressure is essential and negative pressures would imply phloem failure [86]. This behavior highlights the central role of p_m as a control variable in the bifurcation analysis presented later.

The second equation necessary to describe the transport capacity is the conservation of the sucrose mass within the phloem. Formally, this equation should be written in both the radial and axial directions. However, because the aspect ratio $\epsilon = r/L$ is very small in the phloem, a one-dimensional approximation similar to that used in the momentum balance can be applied. A major departure from the approximations involved in the momentum balance is the role of advective transport relative to molecular diffusion. Although the flow is at low Reynolds number, the molecular diffusion of sucrose in water is quite small and advective transport is more significant compared to diffusive transport. For this reason, the one-dimensional form is obtained by area-averaging the full advection–diffusion equation as detailed elsewhere [67]. In the present formulation, a local sucrose sink term is added to the area-averaged equation. The sink reflects local sucrose removal into surrounding cells and is included to accommodate the fact that sugars can be removed across the phloem for respiration, anabolism, and storage.

For the purposes of bifurcation analysis, the flow is further assumed to be at steady state leading to

$$\frac{\partial}{\partial x}\left[\left(1 + \underbrace{\frac{r^2}{24D}\frac{\partial u}{\partial x}}_{TD_{\text{advection}}}\right)cu\right] = \frac{\partial}{\partial x}\left[\left(\underbrace{D\frac{r^2u^2}{48D^2}}_{TD_{\text{dispersion}}} + D\right)\frac{\partial c}{\partial x}\right] - \underbrace{\left(\frac{c(x) - c_b}{t_r}\right)}_{Sucrose\ Sink}. \tag{11}$$

where D is the molecular diffusivity (assumed independent of c), c_b is the background sucrose concentration in the surrounding cells, and t_r is the characteristic removal time. The terms labeled $TD_{\text{advection}}$ and $TD_{\text{dispersion}}$ account for Taylor dispersion effects: the former represents the enhancement of advective transport due to velocity gradients arising from osmotically driven radial inflow of water [67], while the latter represents an effective increase in axial diffusion arising from the coupling between shear flow and molecular diffusion in scalar transport. In a closed tube or for impervious walls, $TD_{\text{advection}} = 0$. This assumption cannot be applied to the phloem.

The presence of a sucrose sink along the entire phloem axis has been reviewed elsewhere [18]. It is here described as analogous to a first-order removal process given by $(c - c_b)/t_r$. This

description is analogous to a binding/unbinding process, where a background concentration c_b, which describes the sucrose at the sink, is presumed constant on time scales comparable with the removal time t_r. If t_r is larger than the characteristic transport time of photosynthates along the phloem (for example, for a 1 m crop with an average sap velocity of 100 cm/h, the transport time is around 3600 s), removal is considered slow and the sink term along the phloem is small (standard assumption in common models); conversely, if t_r is smaller than the transport time, sucrose is rapidly depleted. This interpretation can also be obtained from a scaling analysis by comparing the relative importance of the advective term ($\sim uc/L$) to the sink term ($\sim c/t_r$). The dependence on $(c - c_b)$ reflects the inequality between phloem sucrose concentration and neighboring cell demand. When the difference is large, removal is enhanced, whereas when it is small, little sucrose is available for release. Other localized sinks can also be included in future analysis such as those associated with herbivory. Herbivory can introduce localized sinks because sugars accumulate around damaged tissues to support defense responses and repair [22, 82, 102]. For simplicity, c_b and t_r are assumed to be uniform along x, though spatial variation in t_r and c_b could be incorporated within this framework if known. In the present bifurcation analysis, only t_r from the sink term was treated as a control variable since it is more likely to be regulated by the plant through adjustments at the phloem–cell interface.

Equations 10 and 11 form a coupled system of equations for the sought unknowns $p(x)$ and $c(x)$. As both equations are second order in x, two boundary conditions are required for each to obtain a unique solution. For $c(x)$, $c(0) = c_0$ is prescribed to represent loading from leaves, while $c(L) = 0$ reflects the assumption that roots act as very large (infinite here) sinks. For $p(x)$, water potential equilibrium between phloem and xylem is imposed at both ends (i.e. mechanical equilibrium is achieved) with $p|_{x=0} = R_g T c(0) - p_m$ at the leaf and $p|_{x=L} = R_g\ T\ c(L) - p_m\,(1 - L/L) = 0$ at the root (since the concentration is zero at $x = L$). Here, the xylem water potential at the root is assumed to be zero, corresponding to fully saturated soil with negligible root resistance. This represents an idealized boundary condition that can be relaxed in future work by introducing parameters for soil dryness and rhizosphere conductance. In this case, only p_m, which is assumed to be much larger in magnitude than the root-xylem water tension, impacts the phloem. With these boundary conditions specified, the transport problem is fully determined and ready for analysis of transport capacity and bifurcation behavior. Details of the numerical scheme used to solve Equations 10 and 11 and to evaluate $TR(c_0)$ are provided in Appendix B. All variables and constants used in the theoretical formulation are summarized in Table 1.

Here, it is assumed that both supply and transport capacity depend on c_0, the chosen state variable, and the balance between them would provide the equilibrium concentrations c_0^* and a basis for identifying under which conditions/control variables the phloem fails. Among the environmental control variables, leaf water potential p_m plays a central role. It governs marginal water-use efficiency and, in turn, constrains carbon assimilation [42, 56, 65]. Structural controls include the phloem length L (i.e. plant height) and radius r, while physiological controls are captured by the sink strength, represented by the removal time t_r. The governing dynamics may be written in reduced form as

$$\frac{dc_0}{dt} = PR(c_0) - TR(c_0) = f(c_0), \tag{12}$$

For each control variable set, $PR(c_0)$ and $TR(c_0)$ are solved numerically: assimilation is first computed from stomatal optimality theory at the imposed p_m, with down-regulation at high c_0 to account for feedback inhibition; transport is then obtained from the PFH by solving the coupled water and solute equations along the discretized phloem axis. The total transport rate $TR(c_0)$ is calculated as the mean sucrose flux multiplied by the combined cross-sectional

area of all phloem elements P_a.

Equilibria are given by $f(c_0^*) = 0$, or equivalently $PR(c_0^*) = TR(c_0^*)$. Their stability depends on the local slope $f'(c_0^*)$: if $f'(c_0^*) < 0$, perturbations around c_0^* decay and the equilibrium is stable; if $f'(c_0^*) > 0$, perturbations amplify and the equilibrium is unstable [92]. In situations where $f'(c_0^*) = 0$, higher-order terms in the expansion of $f(c_0)$ must be retained to determine stability.

This bifurcation framework allows for the analysis of phloem resilience. Functional transport corresponds to stable equilibria where photosynthetic supply and phloem transport remain in balance, while failure is defined by the loss of such equilibria or by trajectories that cross into the unstable domain. Using both environmental factors and structural traits for this analysis, it is possible to identify the ranges of the control variables that sustain sucrose transport and those that result in catastrophe. In this way, bifurcation analysis translates the coupling of photosynthesis, plant hydraulics, and phloem loading into a set of critical thresholds that can be directly compared across scenarios. The numerical results presented below map out these bifurcations under realistic ranges of leaf water potential, conduit geometry (length and radius), and sink strength (mainly through t_r), thereby illustrating how environmental stress, plant form, and plant physiology jointly govern phloem vulnerability.

2.3 Environmental Drivers and Parameter Specification

In the model calculations reported here, a number of assumptions were made about the environmental drivers, photosynthetic parameters, and phloem properties. The atmospheric carbon dioxide concentration was set to $c_a = 400$ ppm with leaves experiencing a mean photosynthetically active radiation $I = 800$ μmol m^{-2} s^{-1}, a mean air temperature of 25 ^{o}C, and a relative humidity of 40 %. The high I here implies that photosynthesis is limited by RuBisCO. The photosynthetic parameters are: the maximum rate of RuBP carboxylation capacity catalyzed by Rubisco $V_{c,\max} = 59$ μmol m^{-2} s^{-1}, the minimum marginal water use efficiency $\lambda_{0,\min} = 50$ mmol mol^{-1} kPa^{-1}, the compensation point $c_p = 40$ ppm, the Michaelis-Menten constants for oxygen fixation $K_{c,o} = 300$ ppm and for oxygen inhibition $K_{o,a} = 300$ mmol/mol, the atmospheric oxygen concentration $C_{o,a} = 210$ mmol/mol, and the apparent quantum yield for electron transport coefficient $\alpha_p = 0.064$ mol electron/mol photon. In the description of the down-regulation of photosynthesis, $\alpha = 1200$ mol/m^3 and $\delta = 1600$ mol/m^3 were adopted from [71], which represents the range where sucrose viscosity becomes significant. The cross-sectional area of all phloem tubes within a stem/trunk of any length was set to $P_a = 0.000825$ m^2 and the overall leaf area per individual plant to $L_a = 32.5$ m^2. The membrane permeability k was set to 10^{-14} m Pa^{-1} s^{-1}. The sucrose molecular diffusivity D in water weakly decreases with increasing c_0. In terms of the dynamically relevant quantity to the transport equations, the Schmidt number dependence ($=\nu/D$) on increasing c_0 is governed by the rapidly increasing ν than the weakly decreasing D. For this reason, D was set to a constant of 4×10^{-10} m$^2/s$. The temperature of the sap was assumed to be constant at $T =$ 298 K, and the ideal gas constant is $R_g = 8.314$ J mol^{-1} K^{-1}. Unless otherwise stated, the tube length is set to $L = 10$ m and its radius is set to $r = 10$ μm. Here, L is approximated by the plant height.

3 Results

3.1 Local Phloem Dynamics Under Varying Physiological Conditions

The modeled steady state profiles of pressure, axial velocity, and concentration illustrate how transport responds to the two key physiological control variables, leaf water tension p_m and

removal time t_r. Geometric variables, such as L and r, can be studied through their effect on dimensionless numbers and have been explored extensively in previous studies [36, 67, 97]. By contrast, p_m and t_r introduce new terms into the governing equations, broadening their impact beyond typical flow dynamics (e.g. ratios of axial to radial resistance or advective to diffusive transport). These terms also allow evaluation of how physiological and environmental conditions shape flow profiles and transport efficiency.

Figure 1 shows the aforementioned steady state profiles of $c(x)$, $u(x)$, and $p(x)$ along the phloem pathway (x) for varying t_r (left panels) and p_m (right panels). The effect of t_r on transport is generally small except under very fast removal time ($t_r = 1$ s). In this case, $c(x)$ is nearly depleted along the pathway, indicating instantaneous sucrose removal at the sink. The sharp concentration gradient near the source leads to an increase in pressure gradient and in turn u. As for the magnitude of the pressure, decreasing t_r leads to a decrease in p, consistent with the reduction in inflow of water when the amount of sucrose is depleted fast.

In contrast to t_r, variations in p_m exert stronger effect on phloem dynamics (Figure 1, right panels). As p_m increases, pressure near the source decreases and eventually becomes negative, indicating loss of turgor and incipient phloem failure. This decline in pressure is accompanied by a reduction in u, which approaches zero or becomes negative at high p_m (also indicative of phloem failure). The concentration profiles, however, are less sensitive to changes in p_m. At elevated leaf water tension, the profiles appear less diffusive, reflecting stagnation of sucrose when flow collapses. This behavior contrasts with low p_m, where the concentration front propagates along the conduit and sucrose is effectively delivered to the sink.

The combined influence of p_m and t_r is summarized by the front velocity v_f. The v_f is defined as the axially averaged sucrose flux, combining both advective and diffusive/dispersive contributions including the Taylor dispersion effects, normalized by the loading concentration c_0 (Equation 11) and is shown in Figure 2. In this formulation, the effective flux is expressed as an equivalent advective flux, $J_{eff} = v_f c_0$, where v_f represents a steady-state measure for the effective transport velocity within the functional phloem. At low c_0, v_f decreases sharply with increasing p_m and becomes negative when $p_m > 1$ MPa, indicating collapse of phloem transport. In this regime, water tension is the dominant control, whereas variation in t_r has little effect on v_f.

At intermediate c_0, the effect of increasing t_r becomes evident. The v_f increases with increasing t_r (Figure 2) or increases with a reduction in the sucrose sink. This may appear inconsistent with the $u(x)$ in Figure 1, where lower t_r initially produced higher local velocities. Those elevated increases in $u(x)$, featured in Figure 1, were confined to the source region. Thus, when averaged along the entire conduit length, higher t_r generates greater overall averaged u.

At high c_0, transport failure does not occur even under high p_m, as the elevated sucrose concentrations are sufficient to maintain positive pressure and sustained flow. These results are used to motivate the bifurcation analysis that follows.

3.2 Bifurcation Analysis of Physiological Parameters

Figure 3 summarizes the bifurcation analysis for the two physiological control variables under consideration: t_r and p_m. To illustrate how equilibrium points are determined, Figures 3a and 3b separately present the transport capacity (i.e. TR) and production rate (i.e. PR) curves along with their intersections. These intersections define the equilibrium sucrose concentrations c_0^*. Figures 3c and 3d feature the corresponding bifurcation diagrams where the inferred c_0^* resulting from intersections of TR and PR are classified as stable (blue), unstable (green), or stable but associated with phloem failure (red). In all cases, TR increases with c_0, reaches a peak around 1000–1250 mol/m^3, and then decreases as the non-linear viscosity

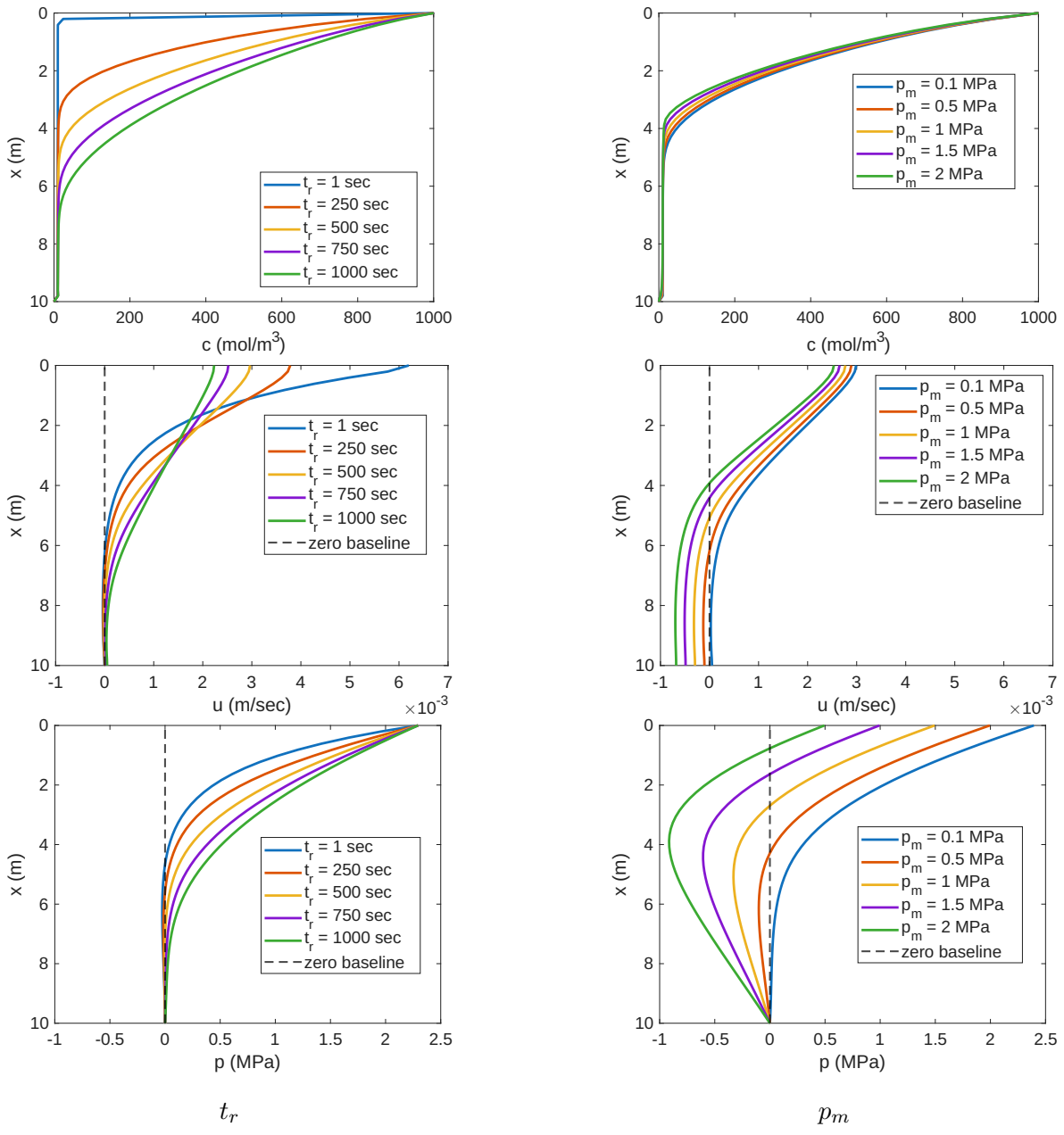

Figure 1: Steady-state longitudinal profiles of sucrose concentration $c(x)$ (top panel), axial velocity $u(x)$ (middle panel), and pressure $p(x)$ (bottom panel) along the phloem pathway for simulations with varying removal time t_r (left panels) and maximum background pressure p_m (right panels). Simulations were conducted with a loading concentration $c_0 = 1000$ mol/m^3, phloem length $L = 10$ m, and phloem radius $r = 10$ μm. A $u < 0$ or a $p < 0$ indicate phloem failure.

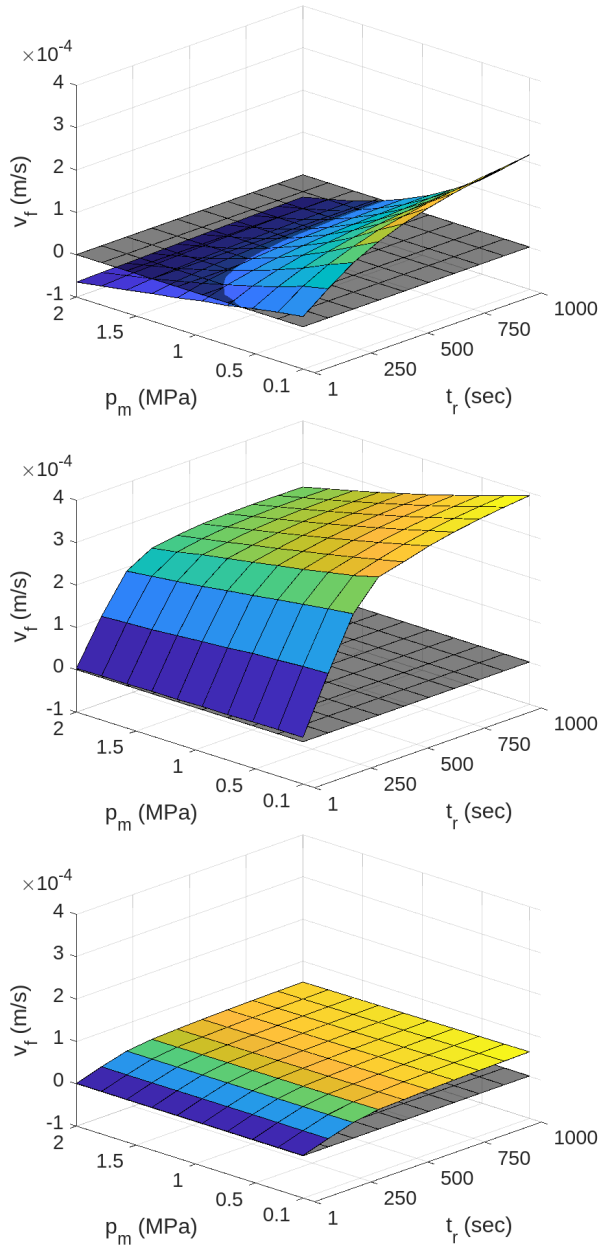

Figure 2: Front velocity v_f as a function of removal time t_r and maximum background pressure p_m, shown for three loading concentrations: $c_0 = 250$ (top), 1000 (middle), and 1750 mol/m^3 (bottom). The front velocity is defined as the axially averaged sucrose flux normalized by c_0 (Equation 11), with $v_f < 0$ indicating phloem failure. All model calculations assume plant height $L = 10$ m and radius $r = 10$ μm. Interestingly, the v_f values computed here are in the same order of magnitude as those reported experimentally at 0.3-3$\times 10^{-4}$ m/s for short crops [4].

effects become limiting. At low c_0, the rise in TR is quasi-linear with increasing concentration, consistent with the Van't Hoff formulation when viscosity changes are small. At higher c_0, TR is strongly reduced and equilibria shift toward failure. Increasing t_r generally widened the separation between equilibrium points, while increasing p_m reduced both TR and PR and lowered the peak transport rate. A further observation is that the equilibrium points near 1250 mol/m^3 coincide with the concentrations associated with maximum TR but also approach the limit where elevated c_0 begins to reduce PR with further increases in c_0. This overlap highlights the sensitivity of the transport system when the phloem is operating at maximum TR.

The bifurcation diagram in Figure 3c illustrates the impact of p_m on the equilibrium points. The violet shaded region marks the observed range of c_0 reported across many species [39] covering passive and active loading into the phloem. This range is presented here as a plausibility check on model outcomes. The orange region denotes loading concentrations where elevated c_0 begins to suppress leaf photosynthesis and PR. At very low p_m, the only equilibrium lies at high sucrose concentrations (on the red branch), corresponding to phloem failure. Once p_m exceeds about 0.4 MPa, however, the lower stable branch shifts downward into the observed c_0 range, producing viable equilibria within reported physiological values. At the same time, the unstable branch (green) moves upward, entering the zone where PR is suppressed at high concentrations, while the red stable branch remains associated with dysfunctional operation well above the observed range of sucrose concentrations. This behavior shows that while increasing p_m reduces the maximum TR, it also separates stable and unstable equilibria more distinctly and relocates the lower stable branch into a plausible operating regime. Because the analysis suggests that increasing p_m leads to 1 (stable) and 3 equilibrium c_0 values (2 stable and 1 unstable), the bifurcation is technically labeled as super-critical pitch-fork. With the highest equilibrium c_0 being stable and unaltered by p_m, the true nature of this bifurcation is a saddle-node at the tangent intersections of TR and PR in which two equilibria collide and annihilate each other as p_m decreases or are created from nothing as p_m increases [92].

The bifurcation diagram in Figure 3d explores the effect of varying t_r on equilibrium sucrose concentrations. At low t_r (i.e. rapid sucrose removal), no functional equilibria were available, and the system converged to the stable high-concentration equilibrium on the red branch (associated with failure). In this case, rapid sink activity reduced the osmotic potential in the phloem, lowering TR (Figure 3b) such that no intersections existed except at very high c_0. Once t_r exceeded a threshold of approximately 400 s, sucrose removal along the pathway was sufficiently reduced to generate a saddle–node-like bifurcation, similar to the p_m case. A stable equilibrium (blue) then emerged independently of the precise value of t_r, operating at concentrations near those associated with maximum TR and within the empirically observed range of c_0. At the same time, an unstable equilibrium (green) appeared at higher concentrations, overlapping with the orange shaded region where elevated c_0 begins to suppress PR. The upper stable branch (red) corresponded to loading concentrations beyond the observed range, where both TR and PR are drastically reduced and the phloem is deemed dysfunctional. Like before, the 'normal form' associated with this bifurcation diagram is a saddle-node bifurcation [92].

Figure 4 combines t_r and p_m as joint control parameters with equilibrium concentrations forming continuous surfaces classified as stable (blue), unstable (green), or stable but dysfunctional (red). This figure shows that phloem failure resembles a cusp catastrophe [112] much like xylem cavitation [40]. At low p_m and short t_r, no functional equilibria occur within the observed physiological range, and solutions lie only on the red surface corresponding to phloem failure. As p_m increases or t_r becomes longer, the blue stable surface extends into the physiologically relevant range of c_0, while the green unstable surface separates it from

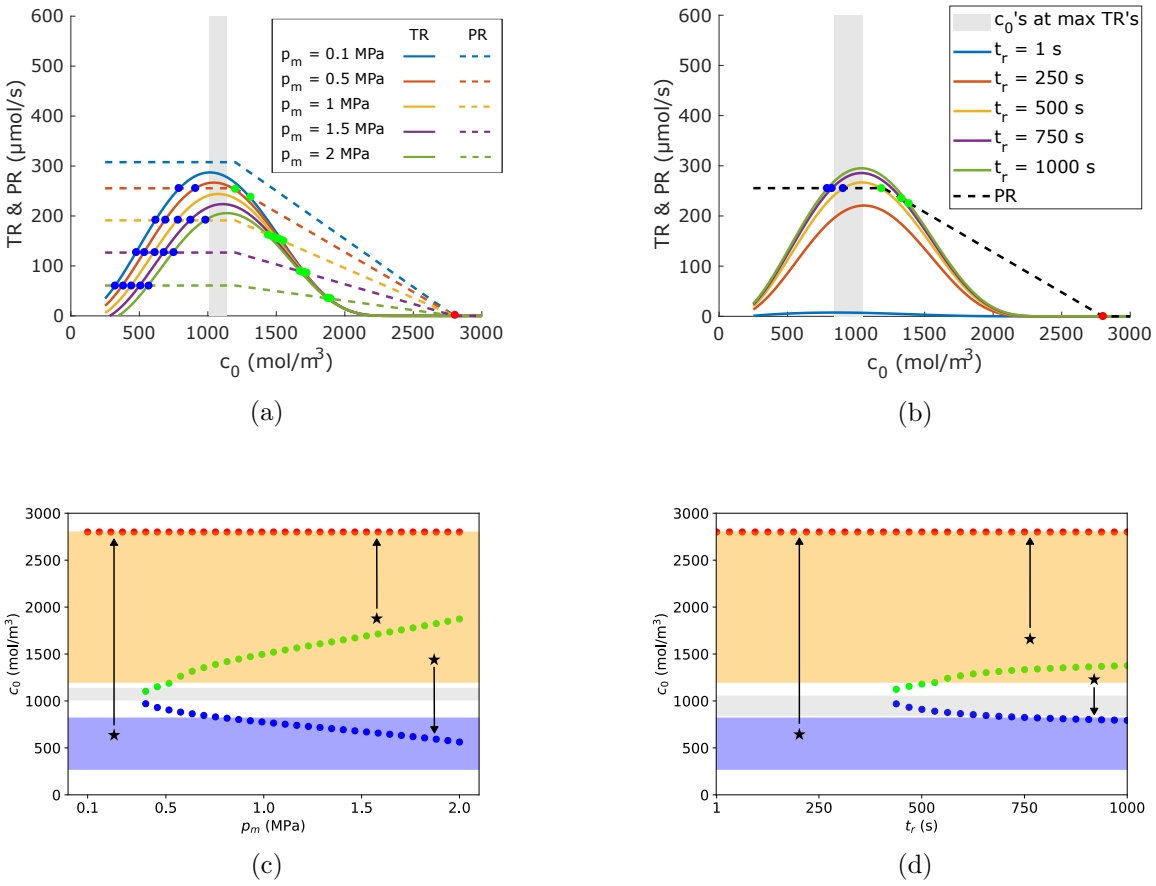

Figure 3: Transport capacity TR (solid lines) and production rate PR (dashed lines) as functions of sucrose loading concentration c_0 for varying maximum background pressure p_m (a) and removal time t_r (b). Intersections of TR and PR curves define equilibrium loading concentrations c_0^*. The corresponding bifurcation diagrams are shown for p_m (c) and t_r (d), where equilibria are classified as stable (blue), unstable (green), or stable but associated with phloem failure (red). Violet shaded regions denote observed c_0 values reported in the literature, orange shaded regions indicate concentrations where elevated c_0 suppresses PR, and the grey shaded regions are the c_0 values at which maximum TR occurred across the different parameter sets. All model calculations assume phloem length $L = 10$ m and radius $r = 10$ μm.

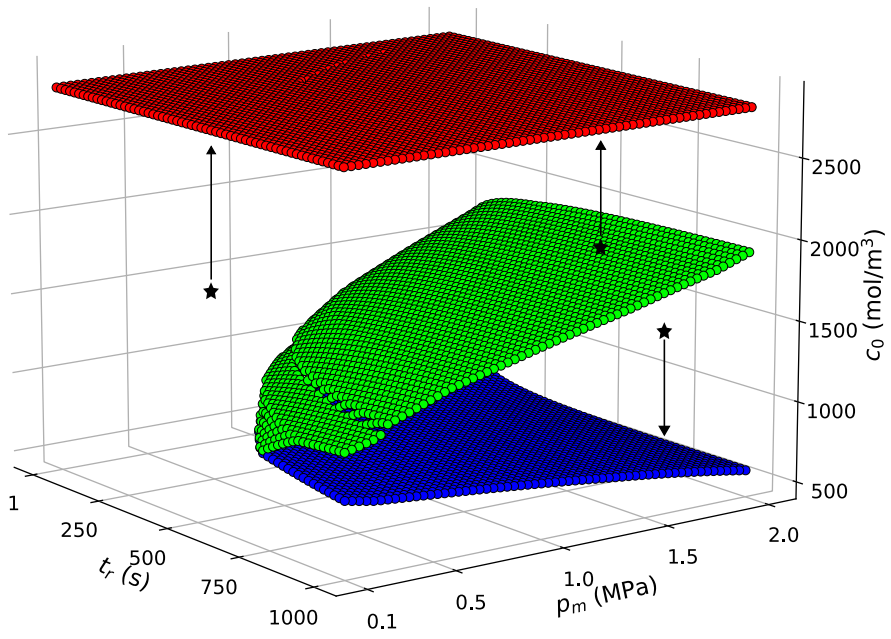

Figure 4: Two-parameter bifurcation diagram showing equilibrium sucrose concentrations c_0 obtained when transport capacity TR equals production rate PR, as a function of removal time t_r and maximum background pressure p_m. Equilibria are classified as stable (blue), unstable (green), or stable but associated with phloem failure (red). All model calculations assume phloem length $L = 10$ m and radius $r = 10$ μm.

the red failure surface. The structure of Figure 4 can be understood as a generalization of the two–dimensional bifurcation diagrams. A vertical slice at fixed p_m would reproduce the t_r bifurcation pattern, with a lower stable branch, an intermediate unstable branch, and an upper stable branch at high c_0. Conversely, a slice at fixed t_r would reproduce the p_m bifurcation, where increasing background pressure shifts the stable equilibrium into the observed concentration range while the unstable branch rises toward higher c_0. In this way, the three-dimensional surface shows how the effects of sink activity and water tension combined, delineating the regions of viable transport from those where phloem operation collapses (i.e. a catastrophe).

3.3 Bifurcation Analysis of Geometric Parameters

Figure 5 presents the bifurcation analysis for the two geometric control variables, tube length L and sieve tube radius r. Figures 5a and 5b show transport capacity TR and production rate PR curves with their intersections defining equilibrium sucrose concentrations c_0^*. Figures 5c and 5d show the corresponding bifurcation diagrams, where equilibria are classified as before. The TR curves follow the same generic rise–peak–decline pattern already discussed for the physiological variables, and the analysis here focuses on how geometric scaling modifies the equilibrium structure.

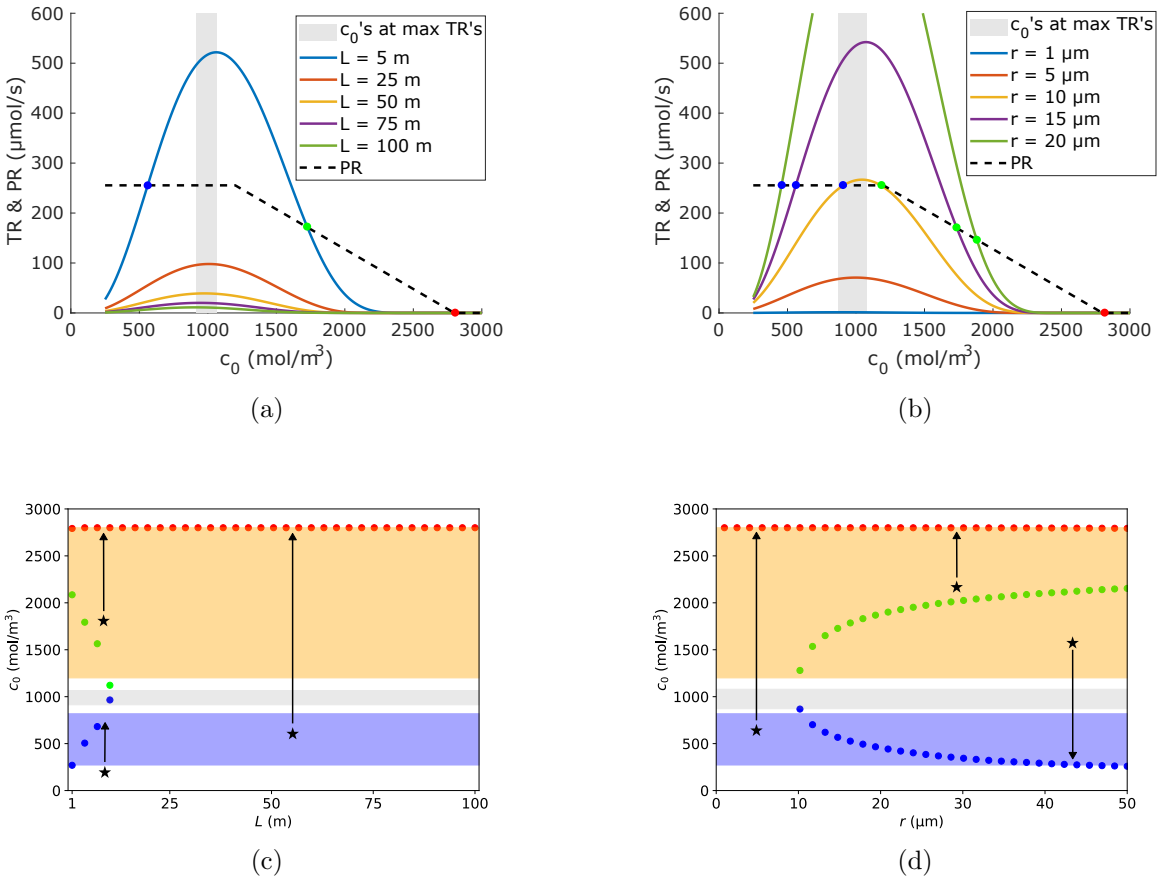

Figure 5: Transport capacity TR and production rate PR as functions of sucrose loading concentration c_0 for varying phloem length L (a) and radius r (b). Intersections of TR and PR curves define equilibrium loading concentrations c_0^*. The corresponding bifurcation diagrams are shown for L (c) and r (d), where equilibria are classified as stable (blue), unstable (green), or stable but associated with phloem failure (red). Violet shaded regions denote observed c_0 values reported in the literature, orange shaded regions indicate concentrations where elevated c_0 suppresses PR, and the grey shaded regions are the c_0 values at which maximum TR occurred across the different parameter sets. All model calculations assume maximum background pressure $p_m = 0.5$ MPa and removal time $t_r = 500$ s.

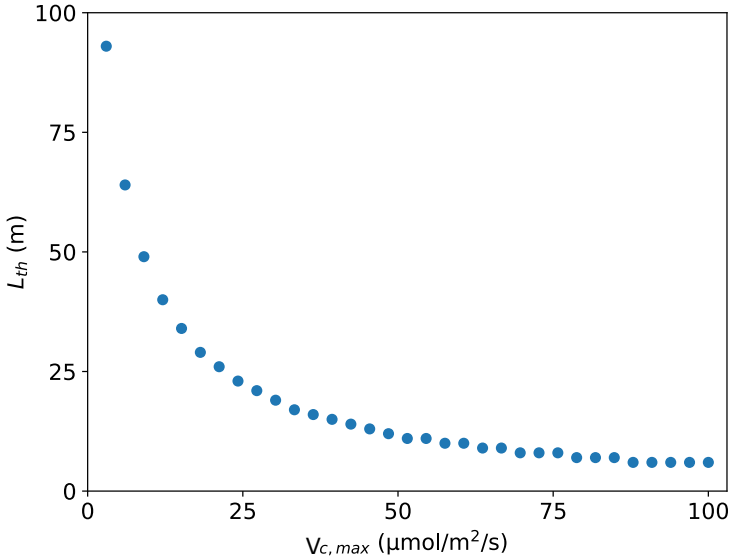

Figure 6: The modeled relation between the threshold phloem length L_{th}, defined as the maximum tube length permitting equilibrium between transport capacity TR and production rate PR, and the maximum carboxylation capacity $V_{c,\max}$ controlling PR. All other parameters are held constant: phloem radius $r = 10$ μm, maximum background pressure $p_m = 0.5$ MPa, and removal time $t_r = 500$ s.

The effect of tube length or plant height variations on phloem failure is analyzed in Figures 5a and 5c. For long tubes ($L > 5$ m), TR declined more strongly than PR such that no equilibrium points existed below approximately 2750 mol/m^3. In this regime, PR consistently exceeded TR, leading to a positive imbalance between production and transport and causing c_0 to increase continuously. This accumulation resulted in clogging of the pathway and ultimately phloem failure. These findings imply that the PR values assumed in the model are unrealistically high for plants with large L. In particular, the high $V_{c,max}$ used in the calculation of A is comparable to values reported for shrubs and grasses instead of tall trees. Additional model calculations that vary $V_{c,max}$ featured in Figure 6 showed that the maximum acceptable length for safe transport, L_{th}, increased as $V_{c,\max}$ decreased when all else is equal. This analysis suggests that a reduction of $V_{c,max}$ by a factor of two would lower A (and PR) sufficiently to restore the balance between reduced transport capacity due to longer L and photosynthetic supply. Under these conditions, equilibrium c_0 values were consistent with the range reported in the literature (violet shaded regions in all figures). This effect of lower $V_{c,max}$ extends beyond L: any reduction in PR shifts the stable equilibrium (blue branch) toward smaller c_0^* values, moving further into the observed range of sucrose concentrations reported in the literature.

The effect of decreasing sieve tube radius on phloem failure is analyzed in Figures 5b and 5d. For narrow tubes ($r < 10$ μm), TR was too small to allow intersections with PR except at very high c_0. In this case, only one equilibrium value is obtained and is featured on the red stable branch. This outcome is consistent with the Hagen-Poiseuille formulation, which shows that the volumetric flow rate is proportional to r^4/μ, where μ increases sharply with increased sucrose concentration. Thus, a smaller cross-sectional area both reduces flow capacity and requires higher c_0, which in turn elevates viscosity and increases frictional losses faster than the osmotic potential rises (linear in c). As the radius increased to around 10 μm,

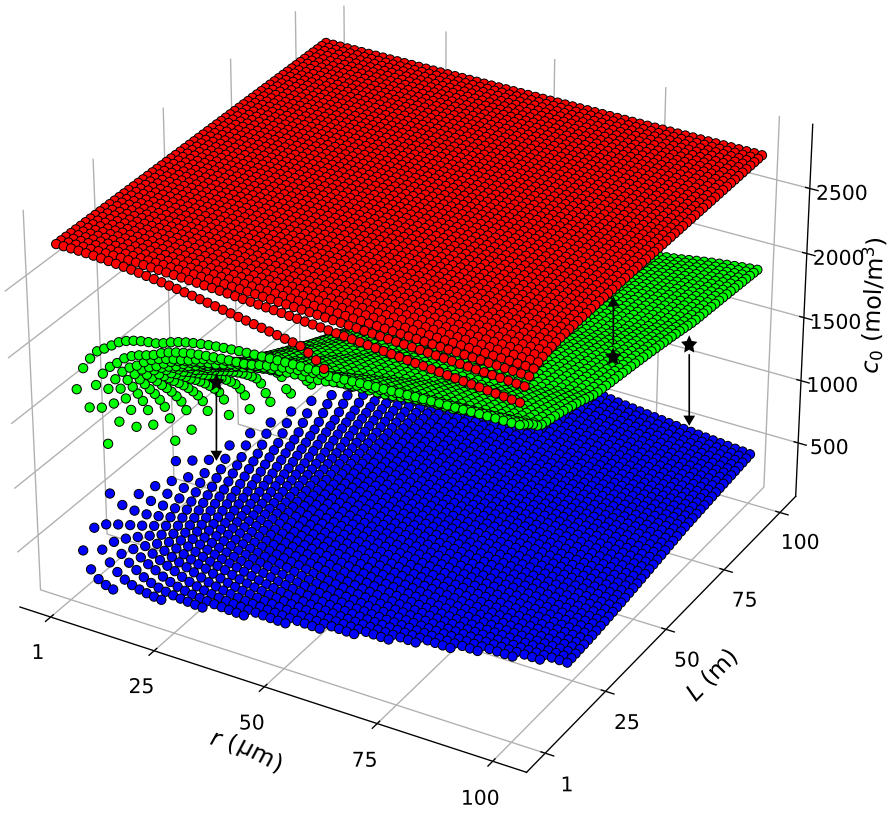

Figure 7: Two-parameter bifurcation diagram showing equilibrium sucrose concentrations c_0 obtained when transport capacity TR equals production rate PR, as a function of phloem length L and radius r. Equilibria are classified as stable (blue), unstable (green), or stable but associated with phloem failure (red). All model calculations assume maximum background pressure $p_m = 0.5$ MPa and removal time $t_r = 500$ s.

two new equilibrium points appeared, one stable and one unstable, as before (i.e. a saddle node bifurcation). For the stable equilibrium, the concentration decreased gradually with increasing r, remaining within the observed range of c_0, while the unstable branch trended upward into the region where PR is reduced by feedback at elevated c_0. This trend began to flatten at larger radii, such that increasing r beyond 0.4×10^{-4} m provided little additional hydraulic benefit in terms of transport efficiency. However, wider radii did confer some safety advantage by elevating the unstable equilibrium branch and its associated bifurcation point, thereby shifting the threshold for collapse to higher sucrose concentrations.

Figure 7 combines L and r as joint control parameters with equilibrium concentrations c_0 forming continuous surfaces classified as stable (blue), unstable (green), or stable but dysfunctional (red). As in Figure 4, the shape of this surface is suggestive that phloem failure resembles a cusp catastrophe. For long tubes (or tall plants) and narrow radii, no functional equilibria occurred within the observed physiological range, and c_0 solutions lay only on the red surface corresponding to phloem failure. As r increased or L decreased, the blue stable surface extended into the physiologically relevant range of c_0, while the green unstable surface separated it from the red failure surface. Once again, the structure of Figure 7 can be understood as a generalization of the two–dimensional bifurcation diagrams, showing how tube length (surrogate for plant height) and tube radius interact to delimit the regions

of viable transport from those where failure occurs.

4 Discussion and Conclusion

The balance between sucrose production from photosynthesis PR and the transport capacity of the phloem TR was analyzed within a bifurcation framework to identify the physiological and structural parameters that govern phloem resilience. The PR was derived from a stomatal optimality hypothesis with externally imposed feedback inhibition at high loading concentrations. The TR was modeled from the steady-state pressure–flow hypothesis in a one-dimensional formulation. The bifurcation framework revealed how this balance between production and transport capacity determines the number and stability of equilibrium loading concentration states. Two physiological controls not previously incorporated in such models were considered. These two control variables are the maximum background pressure p_m, representing leaf water tension, and the removal time t_r, representing sink strength along the phloem. Increases in p_m simultaneously reduced PR and TR, lowering flow velocity and increasing the likelihood of failure, while longer t_r sustained osmotic gradients and enhanced overall stability.

Beyond the local effects of these control variables on phloem dynamics, stability analysis was performed on these variables with two additional geometric parameters, tube length L and radius r. Depending on parameter values, the phloem failure was shown to be characterized by a cusp catastrophe. This catastrophe exhibits either a single (catastrophic) equilibrium or a saddle–node bifurcation totaling to three equilibria: two stable (one functional and one catastrophic) and one unstable. The upper stable equilibrium at high c_0 reflected a dysfunctional state, as high concentrations elevate viscosity and stagnate flow. The unstable equilibrium typically occurred in the range where elevated c_0 suppressed photosynthesis, while the lower stable equilibrium fell within the functional values reported in the literature. Importantly, the phloem was never predicted to operate at the c_0 that maximizes TR; instead, plants appear to sacrifice some efficiency in favor of safety, maintaining their operational sucrose concentration below the unstable branch. This safety–efficiency trade-off suggests a fundamental hydraulic strategy in which some robustness is prioritized over maximum transport efficiency.

The analysis also revealed a surprising coordination between photosynthetic capacity ($V_{c,max}$) and phloem path length. For tall trees, maintaining a viable equilibrium requires (counterintuitively) a reduction in PR to match the diminished TR imposed by long-distance transport or L. This coordination is consistent with empirical evidence that trees operate with lower maximum carboxylation capacity $V_{c,max}$ than grasses, crops, and shrubs. The empirical evidence rests on a number of $V_{c,max}$ compilation and remote sensing data products [12] that report a mean $V_{c,max}$ for (1) crops to be 88 μmol m^{-2} s^{-1}, (2) grasses to be 75, (3) shrubs to be 59, (4) evergreen broad leaf forests to be 47, (5) deciduous needle leaf forests to be 44, (6) deciduous broad leaf forests to be 44, and (7) evergreen needle leaf forests to be 32. That is, high $V_{c,max}$ values typical of crops, grasses, or shrubs would overwhelm the reduced TR associated with increased plant height (i.e. increased flow resistance with increasing L), forcing the phloem into a dysfunctional state. By contrast, the reduced $V_{c,max}$ observed in forests lowers PR sufficiently to maintain viable intersections between PR and TR, thereby sustaining transport when all else is the same.

Model results further showed that when $V_{c,max}$ exceeded about 40 μmol m^{-2}s^{-1}, sensitivity to increasing phloem length diminished, whereas for $L > 25$ m an inverse relation between $V_{c,max}$ and L emerged. The $V_{c,max}$ of plants is impacted by a plethora of factors such as available nutrients (leaf nitrogen and phosphorous), leaf water potential, specific leaf area, among others [73, 108]. Hence, direct quantitative comparisons between $V_{c,max}$ and L will likely be masked by other local factors (e.g. irrigation, fertilization or N deposition, etc...). Nonethe-

less, the work here shows that reductions in TR caused by increased L requires reductions to PR (not increases) within a certain range of plausible c_0 values.

This coordination between photosynthetic supply and transport capacity likely extends to other traits beyond $V_{c,\max}$. For example, adjusting the parameters in Equation 5 would similarly reduce photosynthetic supply and help recover phloem hydraulic function. Coordination is also expected between the parameters controlling photosynthetic supply and the sink removal rate t_r, which represents plant demand along the stem. Furthermore, anatomical coordination is likely, as taller trees may require wider phloem conduits to increase sieve element conductivity and thereby permit higher $V_{c,\max}$ without inducing phloem failure. This expectation is consistent with empirical observations showing that phloem conduit radius scales positively with tree size [50, 83].

The ecological significance of water tension follows directly from the bifurcation structure. At low p_m, the model predicted phloem failure because PR exceeded TR, producing only a high c_0 equilibrium. In reality, plants do not fail at such modest water tensions, suggesting that photosynthetic capacity is downregulated more than represented here through adjustments in stomatal conductance or other biochemical constraints to keep PR and TR in balance. As p_m increased, two equilibrium points emerged and the separation between them widened, effectively increasing the hydraulic safety margin. This behavior helps explain why the stable equilibria revealed by the model align with empirical c_0 values across species, and why phloem transport can remain functional under moderate drought despite reductions in efficiency. Overall, the analysis underscores the need to consider dynamic feedbacks in photosynthesis when linking leaf water status to vascular stability, while highlighting the robustness of the phloem system across a range of water potentials.

Several study limitations should also be acknowledged. The present framework assumes steady state, whereas plants operate dynamically across multiple timescales, with fluctuations in photosynthesis, transpiration, and loading/unloading over minutes to hours. While the steady state approach is a logical starting point for locating thresholds and structural constraints, it does not capture transient buffering, feedbacks, and recovery that likely shape resilience under a changing environment. In addition, the model assumes that phloem loading depends directly on assimilation, whereas in real plants loading rates are regulated by local concentration gradients and membrane transport processes [7]. The model also ignores the influence of ions, particularly potassium, on phloem function, which can partly decouple osmotic pressure from sucrose concentration [3]. The current analysis is best viewed as a diagnostic tool that reveals the physical and biological limits of phloem operation. This view is in the same spirit as the qualitative analysis usually sought when using bifurcation analysis. Hence, the work here should not be viewed as a complete description of all aspects of phloem dynamics.

Within these constraints, catastrophe theory provides an organizing framework for describing phloem dysfunction. Embedding hydraulic traits, photosynthetic capacity, and sink dynamics within a common bifurcation structure shows how gradual shifts in simplified representations of environmental controls, such drought-induced decreases in xylem water potential represented by p_m, or biotic stressors such as pest or pathogen attacks that alter sink removal rates represented by t_r, as well as phloem structural controls can precipitate sudden transport collapse. In doing so, it highlights both the robustness of phloem function under moderate stress and the vulnerabilities that emerge under extremes. Extending this framework to dynamic models that explicitly couple leaf photosynthesis, xylem water transport, and phloem loading–unloading dynamics will be essential for quantifying how plants navigate the safety–efficiency trade-off under fluctuating conditions. Such advances will refine mechanistic understanding of vascular resilience and improve predictions of plant survival, productivity, and the stability of forest carbon cycling under drought and warming scenarios.

Acknowledgments

MN acknowledges the startup support from the Lebanese-American University; GK acknowledges support from the U.S. National Science Foundation (NSF-AGS-2028633) and the U.S. Department of Energy (DE-SC-0022072); SS acknowledges support from U.S. Department of Defense, Strategic Environmental Research and Development Program (SERDP) grant RC25-0189.

Data Availability

The model code and scripts used in this study are available at: 10.5281/zenodo.17859318

Author Contributions

LY Model development; Analysis; Visualization; Writing - Original Draft; Writing- Review and Editing
MN Conceptualization; Analysis; Writing - Original Draft; Writing - Review and Editing
JCD Analysis; Writing - Review and Editing
SS Analysis; Writing - Review and Editing
GK Conceptualization; Methodology; Analysis; Writing - Review and Editing

A A Linear Stomatal Optimality Theory

For illustration purposes, a linearized form of the static stomatal optimality solution for photosynthesis is presented. The full formulation, which accounts for additional biochemical and diffusional constraints, is used in the bifurcation analysis of PR and is detailed elsewhere [42]. The linearized version is retained here because it preserves the same parameter structure while providing a transparent analytical form [42, 70, 72]. Also, the linearization adopted here is expected to be plausible when RuBisCO limits A. The assimilation rate can be expressed as

$$A = \frac{\beta_1 c_a}{\beta_2 + \beta_3 c_a}\left(1 - \sqrt{\frac{1.6\,\mathrm{VPD}}{c_a}\,\lambda}\right), \tag{13}$$

where c_a is the atmospheric CO_2 concentration, VPD is, as before, the vapor pressure deficit, and λ is the marginal water-use efficiency. The coefficients β_1 and β_2 depend on the photosynthetic limitation regime, while $\beta_3 = c_i/c_a \in [0.7, 0.9]$ represents the long-term intercellular to ambient CO_2 ratio for C3 plants (set as constant in the linearization).

The maximum value of λ that permits finite assimilation is obtained by setting the square-root term in Eq. (13) to zero:

$$\lambda_{\max} = \frac{c_a}{1.6\,\mathrm{VPD}}. \tag{14}$$

For the bifurcation analysis, λ is assumed to increase linearly with leaf water tension (p_m):

$$\lambda = \lambda_{\min} + \frac{p_m}{3}\left(\lambda_{\max} - \lambda_{\min}\right), \tag{15}$$

where $\lambda_{\min}$ and $\lambda_{\max}$ correspond to maximum stomatal opening and complete closure, respectively. More complex λ functions, including those predicted from dynamic optimality theories [65], can be adopted.

The parameters β_1 and β_2 depend on whether photosynthesis is RuBisCO- or RuBP-limited:

- **RuBisCO limitation:** β_1 is the maximum carboxylation capacity $V_{c,\max}$, while

$$\beta_2 = K_{c,o}\left(1 + \frac{C_{o,a}}{K_{o,a}}\right), \tag{16}$$

where $K_{c,o}$ and $K_{o,a}$ are the Michaelis constants for CO_2 fixation and oxygen inhibition, and $C_{o,a}$ is the oxygen concentration in air. All three are temperature dependent and can be treated as constants for a given species and temperature.

- **RuBP limitation:** β_1 is linked to the photosynthetically active radiation (I) using a leaf absorptivity to photosynthetically active radiation ($= 0.08$) and a maximum quantum efficiency ($= 0.8$) whose product defines an apparent quantum yield $\alpha_p = 0.064$ [10]. It saturates at the maximum electron transport rate $J_{e,\max}$ given by

$$\beta_1 = \frac{\alpha_p I}{\sqrt{1 + (\alpha_p I / J_{e,\max})^2}}. \tag{17}$$

In the RuBP limit, $\beta_2 = 2c_p$ with c_p being the CO_2 compensation point that varies with temperature. Empirical evidence suggests $J_{e,\max}/V_{c,\max} \approx 2$ at 25 °C [108].

In Equation 13, A increases with increasing c_a but saturates at very high $c_a \gg \beta_2/\beta_3$. Increasing atmospheric aridity raises VPD and reduces A, while increasing p_m increases λ and similarly suppresses A, consistent with empirical evidence and predictions from dynamic stomatal optimality theories [55, 56, 65]. For the bifurcation analysis, all environmental parameters (c_a, VPD, radiation, temperature) are held constant, leaving λ—and thus p_m—as the sole bifurcation parameter.

B Numerical Solution of Transport Capacity

The $TR(c_0)$ is obtained by solving the coupled one-dimensional system for pressure $p(x)$ and sucrose concentration $c(x)$ presented in Section 2, namely the water balance (Equation 8), the Hagen–Poiseuille relation (Equation 9), and the sucrose conservation equation including Taylor dispersion and unloading (Equation 11). The xylem water potential is parameterized as a linear decline from 0 MPa at the root ($x = L$) to $-p_m$ at the leaf ($x = 0$). The conduit of length L is discretized into $N = 50$ uniform segments. All derivatives are computed using central finite-difference approximation away from the immediate boundaries. Boundary conditions are imposed as $c(0) = c_0$ (leaf loading) and $c(L) = 0$ (idealized infinite sink at the root) for sucrose, and $p(0) = R_g T c(0) - p_m$, $p(L) = 0$ for pressure, consistent with water potential equilibrium between phloem and xylem.

Because the governing equations are nonlinear, the solution is obtained iteratively using implicit schemes. An initial linear concentration profile $c(x)$ is assumed, from which the pressure field $p(x)$ is computed using Equation 10 and the velocity $u(x)$ from Equation 9. The updated velocity is then used in Equation 11 to calculate a new sucrose profile. The procedure is repeated until the normalized root-mean-square difference (i.e., relative ℓ_2 norm) between successive $c(x)$ profiles falls below 10^{-6}, at which point convergence is declared. Once a converged solution is obtained, the local sucrose mass flux is evaluated as

$$J = \left(1 + \frac{r^2}{24D}\frac{\partial u}{\partial x}\right) cu - \left(\frac{r^2 u^2}{48D^2} + 1\right) D\frac{\partial c}{\partial x}, \tag{18}$$

which includes contributions from advection, molecular diffusion, and Taylor dispersion in the presence of osmosis. The conduit-averaged flux is then multiplied by the total phloem cross-sectional area, P_a, to obtain the transport capacity $TR(c_0)$.

References

[1] E. A. Ainsworth and D. R. Bush. Carbohydrate export from the leaf: a highly regulated process and target to enhance photosynthesis and productivity. *Plant Physiology*, 155 (1):64–69, 2011.

[2] G. Angeles, B. Bond, J. Boyer, T. Brodribb, J. Brooks, M. Burns, J. Cavender-Bares, M. Clearwater, H. Cochard, J. Comstock, et al. The cohesion-tension theory. *New Phytologist*, 163(3):451–452, 2004.

[3] B. A. Babst, D. M. Braun, A. A. Karve, R. Frank Baker, T. M. Tran, D. J. Kenny, J. Rohlhill, J. Knoblauch, M. Knoblauch, G. Lohaus, et al. Sugar loading is not required for phloem sap flow in maize plants. *Nature Plants*, 8(2):171–180, 2022.

[4] O. Biddulph and R. Cory. An analysis of translocation in the phloem of the bean plant using THO, P32, and C14. *Plant Physiology*, 32(6):608–619, 1957.

[5] O. Biddulph and R. Cory. Translocation of C14 metabolites in the phloem of the bean plant. *Plant Physiology*, 40(1):119–129, 1965.

[6] C. Bouchard and B. Granjean. A neural network correlation for the variation of viscosity of sucrose aqueous solutions with temperature and concentration. *LWT-Food Science and Technology*, 28(1):157–159, 1995.

[7] D. M. Braun. Phloem loading and unloading of sucrose: what a long, strange trip from source to sink. *Annual Review of Plant Biology*, 73(1):553–584, 2022.

[8] M. Brunn, B. Hafner, M. Zwetsloot, F. Weikl, K. Pritsch, K. Hikino, N. Ruehr, E. Sayer, and T. Bauerle. Carbon allocation to root exudates is maintained in mature temperate tree species under drought. *New Phytologist*, 235(3):965–977, 2022.

[9] P. Cabrita, M. Thorpe, and G. Huber. Hydrodynamics of steady state phloem transport with radial leakage of solute. *Frontiers in Plant Science*, 4:531, 2013.

[10] G. Campbell and J. Norman. *An introduction to environmental biophysics*. Springer Science & Business Media, 1998.

[11] M. Canny. The rate of translocation. *Biological Reviews*, 35(4):507–532, 1960.

[12] J. Chen, R. Wang, Y. Liu, L. He, H. Croft, X. Luo, H. Wang, N. Smith, T. Keenan, C. Prentice, et al. Global datasets of leaf photosynthetic capacity for ecological and earth system research. *Earth System Science Data*, 14(9):4077–4093, 2022.

[13] G. Collatz, J. T. Ball, C. Grivet, and J. Berry. Physiological and environmental regulation of stomatal conductance, photosynthesis and transpiration: a model that includes a laminar boundary layer. *Agricultural and Forest Meteorology*, 54(2):107–136, 1991. ISSN 0168-1923. doi: 10.1016/0168-1923(91)90002-8.

[14] V. Couvreur, G. Ledder, S. Manzoni, D. A. Way, E. B. Muller, and S. E. Russo. Water transport through tall trees: a vertically explicit, analytical model of xylem hydraulic conductance in stems. *Plant, Cell & Environment*, 41(8):1821–1839, 2018.

[15] I. Cowan and J. Troughton. The relative role of stomata in transpiration and assimilation. *Planta*, 97(4):325–336, 1971.

[16] A. Crafts and O. Lorenz. Fruit growth and food transport in cucurbits. *Plant Physiology*, 19(1):131–138, 1944.

[17] G. Damour, T. Simonneau, H. Cochard, and L. Urban. An overview of models of stomatal conductance at the leaf level. *Plant, Cell & Environment*, 33(9):1419–1438, 2010.

[18] V. De Schepper, T. De Swaef, I. Bauweraerts, and K. Steppe. Phloem transport: a review of mechanisms and controls. *Journal of Experimental Botany*, 64(16):4839–4850, 2013.

[19] R. Dewar, T. Hölttä, and Y. Salmon. Exploring optimal stomatal control under alternative hypotheses for the regulation of plant sources and sinks. *New Phytologist*, 233 (2):639–654, 2022.

[20] H. Dixon and N. Ball. Transport of organic substances in plants. *Nature*, 109(2730): 236–237, 1922.

[21] H. Dixon and J. Joly. On the ascent of sap. *Philosophical Transactions of the Royal Society of London. B*, 186:563–576, 1895.

[22] A. Douglas. Phloem-sap feeding by animals: problems and solutions. *Journal of Experimental Botany*, 57(4):747–754, 2006.

[23] G. Farquhar, S. von Caemmerer, and J. Berry. A biochemical model of photosynthetic CO2 assimilation in leaves of C3 species. *Planta*, 149(1):78–90, 1980.

[24] S. Fatichi, C. Pappas, J. Zscheischler, and S. Leuzinger. Modelling carbon sources and sinks in terrestrial vegetation. *New Phytologist*, 221(2):652–668, 2019.

[25] D. Fensom. Problems arising from a Münch-type pressure flow mechanism of sugar transport in phloem. *Canadian Journal of Botany*, 59(4):425–432, 1981.

[26] D. B. Fisher. An evaluation of the Münch hypothesis for phloem transport in soybean. *Planta*, 139(1):25–28, 1978.

[27] D. Geiger and C. Swanson. Sucrose translocation in the sugar beet. *Plant Physiology*, 40(4):685–690, 1965.

[28] C. Grossiord, S. Sevanto, I. Borrego, A. Chan, A. Collins, L. Dickman, P. Hudson, N. McBranch, S. Michaletz, W. Pockman, et al. Tree water dynamics in a drying and warming world. *Plant, Cell & Environment*, 40(9):1861–1873, 2017.

[29] P. Hari, A. Mäkelä, E. Korpilahti, and M. Holmberg. Optimal control of gas exchange. *Tree Physiology*, 2(1-2-3):169–175, 1986.

[30] S. Henton, A. Greaves, G. Piller, and P. Minchin. Revisiting the Münch pressure–flow hypothesis for long-distance transport of carbohydrates: modelling the dynamics of solute transport inside a semipermeable tube. *Journal of Experimental Botany*, 53 (373):1411–1419, 2002.

[31] T. Hölttä, A. Lintunen, T. Chan, A. Mäkelä, and E. Nikinmaa. A steady-state stomatal model of balanced leaf gas exchange, hydraulics and maximal source–sink flux. *Tree physiology*, 37(7):851–868, 2017.

[32] C. Huang, J. Domec, S. Palmroth, W. Pockman, M. Litvak, and G. Katul. Transport in a coordinated soil-root-xylem-phloem leaf system. *Advances in Water Resources*, 119: 1–16, 2018.

[33] T. Hölttä, H. Mäkinen, P. Nöjd, A. Mäkelä, and E. Nikinmaa. A physiological model of softwood cambial growth. *Tree Physiology*, 30(10):1235–1252, 07 2010. doi: 10.1093/treephys/tpq068.

[34] A. Ives and S. Carpenter. Stability and diversity of ecosystems. *Science*, 317(5834): 58–62, 2007.

[35] K. Jensen. Phloem physics: mechanisms, constraints, and perspectives. *Current Opinion in Plant Biology*, 43:96–100, 2018.

[36] K. Jensen, E. Rio, R. Hansen, C. Clanet, and T. Bohr. Osmotically driven pipe flows and their relation to sugar transport in plants. *Journal of Fluid Mechanics*, 636:371–396, 2009.

[37] K. Jensen, J. Savage, and N. Holbrook. Optimal concentration for sugar transport in plants. *Journal of the Royal Society Interface*, 10(83):20130055, 2013.

[38] K. Jensen, K. Berg-Sørensen, H. Bruus, N. Holbrook, J. Liesche, A. Schulz, M. A. Zwieniecki, and T. Bohr. Sap flow and sugar transport in plants. *Reviews of Modern Physics*, 88(3):035007, 2016.

[39] K. H. Jensen, J. Lee, T. Bohr, H. Bruus, N. Holbrook, and M. Zwieniecki. Optimality of the Münch mechanism for translocation of sugars in plants. *Journal of the Royal Society Interface*, 8(61):1155–1165, 2011.

[40] D. Johnson, G. Katul, and J. Domec. Catastrophic hydraulic failure and tipping points in plants. *Plant, Cell & Environment*, 45(8):2231–2266, 2022.

[41] G. Katul, S. Palmroth, and R. Oren. Leaf stomatal responses to vapour pressure deficit under current and CO2-enriched atmosphere explained by the economics of gas exchange. *Plant, Cell & Environment*, 32(8):968–979, 2009.

[42] G. Katul, S. Manzoni, S. Palmroth, and R. Oren. A stomatal optimization theory to describe the effects of atmospheric co2 on leaf photosynthesis and transpiration. *Annals of Botany*, 105(3):431–442, 2010.

[43] M. Knoblauch, J. Knoblauch, D. Mullendore, J. Savage, B. Babst, S. Beecher, A. Dodgen, K. Jensen, and N. Holbrook. Testing the Münch hypothesis of long distance phloem transport in plants. *Elife*, 5:e15341, 2016.

[44] W. Konrad, A. Roth-Nebelsick, and M. Grein. Modelling of stomatal density response to atmospheric CO2. *Journal of Theoretical Biology*, 253(4):638–658, 2008.

[45] W. Konrad, G. Katul, A. Roth-Nebelsick, and K. Jensen. Xylem functioning, dysfunction and repair: a physical perspective and implications for phloem transport. *Tree Physiology*, 39(2):243–261, 2018.

[46] C. Körner. Paradigm shift in plant growth control. *Current Opinion in Plant Biology*, 25:107–114, 2015.

[47] A. Lang. A relay mechanism for phloem translocation. *Annals of Botany*, 44(2):141–145, 1979.

[48] R. Lemoine, S. Camera, R. Atanassova, F. Dédaldéchamp, T. Allario, N. Pourtau, J. Bonnemain, M. Laloi, P. Coutos-Thévenot, L. Maurousset, et al. Source-to-sink transport of sugar and regulation by environmental factors. *Frontiers in Plant Science*, 4:272, 2013.

[49] R. Leuning. A critical appraisal of a combined stomatal-photosynthesis model for c3 plants. *Plant, Cell & Environment*, 18(4):339–355, 1995.

[50] J. Liesche, M. R. Pace, Q. Xu, Y. Li, and S. Chen. Height-related scaling of phloem anatomy and the evolution of sieve element end wall types in woody plants. *New Phytologist*, 214(1):245–256, 2017.

[51] Y. Liu, M. Kumar, G. Katul, and A. Porporato. Reduced resilience as an early warning signal of forest mortality. *Nature Climate Change*, 9(11):880–885, 2019.

[52] D. Ludwig, D. Jones, C. Holling, et al. Qualitative analysis of insect outbreak systems: the spruce budworm and forest. *Journal of Animal Ecology*, 47(1):315–332, 1978.

[53] G. Manoli, S. Bonetti, J.-C. Domec, M. Putti, G. Katul, and M. Marani. Tree root systems competing for soil moisture in a 3d soil–plant model. *Advances in Water Resources*, 66:32–42, 2014.

[54] G. Manoli, C.-W. Huang, S. Bonetti, J.-C. Domec, M. Marani, and G. Katul. Competition for light and water in a coupled soil-plant system. *Advances in Water Resources*, 108:216–230, 2017.

[55] S. Manzoni, G. Vico, G. Katul, P. Fay, W. Polley, S. Palmroth, and A. Porporato. Optimizing stomatal conductance for maximum carbon gain under water stress: a meta-analysis across plant functional types and climates. *Functional Ecology*, 25(3):456–467, 2011.

[56] S. Manzoni, G. Vico, S. Palmroth, A. Porporato, and G. Katul. Optimization of stomatal conductance for maximum carbon gain under dynamic soil moisture. *Advances in Water Resources*, 62:90–105, 2013.

[57] S. Manzoni, G. Katul, and A. Porporato. A dynamical system perspective on plant hydraulic failure. *Water Resources Research*, 50(6):5170–5183, 2014.

[58] A. Matthews, G. Katul, and A. Porporato. Multiple time scale optimization explains functional trait responses to leaf water potential. *New Phytologist*, 244(2):426–435, 2024.

[59] R. May and G. Oster. Bifurcations and dynamic complexity in simple ecological models. *The American Naturalist*, 110(974):573–599, 1976.

[60] T. J. McCubbin and D. M. Braun. Phloem anatomy and function as shaped by the cell wall. *Journal of Plant Physiology*, 266:153526, 2021.

[61] B. Medlyn, R. A. Duursma, D. Eamus, D. Ellsworth, I. Prentice, C. Barton, K. Crous, P. De Angelis, M. Freeman, and L. Wingate. Reconciling the optimal and empirical approaches to modelling stomatal conductance. *Global Change Biology*, 17(6):2134–2144, 2011.

[62] M. Mencuccini and T. Hölttä. The significance of phloem transport for the speed with which canopy photosynthesis and belowground respiration are linked. *New phytologist*, 185(1):189–203, 2010.

[63] E. Meron. *Nonlinear physics of ecosystems*. CRC Press Boca Raton, FL, 2015.

[64] P. Minchin and A. Lacointe. New understanding on phloem physiology and possible consequences for modelling long-distance carbon transport. *New Phytologist*, 166(3): 771–779, 2005.

[65] A. Mrad, S. Sevanto, J.-C. Domec, Y. Liu, M. Nakad, and G. Katul. A dynamic optimality principle for water use strategies explains isohydric to anisohydric plant responses to drought. *Frontiers in Forests and Global Change*, 2:49, 2019.

[66] E. Münch. *Stoffbewegungen in der Pflanze*. G. Fischer, Jena, Germany, 1930.

[67] M. Nakad, T. Witelski, J.-C. Domec, S. Sevanto, and G. Katul. Taylor dispersion in osmotically driven laminar flows in phloem. *Journal of Fluid Mechanics*, 913:A44001–A44026, 2021. doi: 10.1017/jfm.2021.56.

[68] M. Nakad, J.-C. Domec, S. Sevanto, and G. Katul. Radial–axial transport coordination enhances sugar translocation in the phloem vasculature of plants. *Plant Physiology*, 05 2022. ISSN 0032-0889. doi: 10.1093/plphys/kiac231.

[69] M. Nakad, J.-C. Domec, S. Sevanto, and G. Katul. Toward a realistic representation of sucrose transport in the phloem of plants. *Journal of Geophysical Research: Biogeosciences*, 128(3):e2022JG007361, 2023.

[70] M. Nakad, S. Sevanto, J.-C. Domec, and G. Katul. Linking the water and carbon economies of plants in a drying and warming climate. *Current Forestry Reports*, 9(6): 383–400, 2023.

[71] E. Nikinmaa, T. Hölttä, P. Hari, P. Kolari, A. Mäkelä, S. Sevanto, and T. Vesala. Assimilate transport in phloem sets conditions for leaf gas exchange. *Plant, Cell & Environment*, 36(3):655–669, 2013.

[72] S. Palmroth, F. Berninger, E. Nikinmaa, J. Lloyd, P. Pulkkinen, and P. Hari. Structural adaptation rather than water conservation was observed in scots pine over a range of wet to dry climates. *Oecologia*, 121(3):302–309, 1999.

[73] S. Palmroth, G. Katul, C. Maier, E. Ward, S. Manzoni, and G. Vico. On the complementary relationship between marginal nitrogen and water-use efficiencies among pinus taeda leaves grown under ambient and co2-enriched environments. *Annals of botany*, 111(3):467–477, 2013.

[74] S. Perri, G. Katul, and A. Molini. Xylem–phloem hydraulic coupling explains multiple osmoregulatory responses to salt stress. *New Phytologist*, 224(2):644–662, 2019.

[75] R. Phillips and S. Dungan. Asymptotic analysis of flow in sieve tubes with semipermeable walls. *Journal of Theoretical Biology*, 162(4):465–485, 1993.

[76] H. Poincare. L'Équilibre d'une masse fluide animée d'un mouvement de rotation. *Acta Mathematica*, 7:259–380, 1885.

[77] A. Potkay, A. Cabon, R. Peters, P. Fonti, G. Sapes, A. Sala, A. Stefanski, E. Butler, R. Bermudez, R. Montgomery, et al. Generalized stomatal optimization of evolutionary fitness proxies for predicting plant gas exchange under drought, heatwaves, and elevated CO2. *Global Change Biology*, 31(1):e70049, 2025.

[78] R. Poyatos, V. Granda, V. Flo, M. A. Adams, B. Adorján, D. Aguadé, M. P. Aidar, S. Allen, M. S. Alvarado-Barrientos, K. J. Anderson-Teixeira, et al. Global transpiration data from sap flow measurements: the sapfluxnet database. *Earth System Science Data Discussions*, 2020:1–57, 2020.

[79] Y. Salmon, L. Dietrich, S. Sevanto, T. Hölttä, M. Dannoura, and D. Epron. Drought impacts on tree phloem: from cell-level responses to ecological significance. *Tree Physiology*, 39(2):173–191, 2019.

[80] Y. Salmon, A. Lintunen, A. Dayet, T. Chan, R. Dewar, T. Vesala, and T. Hölttä. Leaf carbon and water status control stomatal and nonstomatal limitations of photosynthesis in trees. *New phytologist*, 226(3):690–703, 2020.

[81] P. Saunders. *An introduction to catastrophe theory*. Cambridge University Press, 1980.

[82] J. Savage, M. Clearwater, D. Haines, T. Klein, M. Mencuccini, S. Sevanto, R. Turgeon, and C. Zhang. Allocation, stress tolerance and carbon transport in plants: how does phloem physiology affect plant ecology? *Plant, Cell & Environment*, 39(4):709–725, 2016.

[83] J. Savage, S. Beecher, L. Clerx, J. Gersony, J. Knoblauch, J. Losada, K. Jensen, M. Knoblauch, and N. Holbrook. Maintenance of carbohydrate transport in tall trees. *Nature Plants*, 3(12):965, 2017.

[84] M. Scheffer, S. Carpenter, J. A. Foley, C. Folke, and B. Walker. Catastrophic shifts in ecosystems. *Nature*, 413(6856):591–596, 2001.

[85] M. Scheffer, J. Bascompte, W. Brock, V. Brovkin, S. Carpenter, V. Dakos, H. Held, E. Van Nes, M. Rietkerk, and G. Sugihara. Early-warning signals for critical transitions. *Nature*, 461(7260):53–59, 2009.

[86] S. Sevanto. Phloem transport and drought. *Journal of Experimental Botany*, 65(7): 1751–1759, 2014.

[87] S. Sevanto. Drought impacts on phloem transport. *Current Opinion in Plant Biology*, 43:76–81, 2018.

[88] S. Sevanto. Flow resistance of phloem sieve plates revisited using an experimental model. *Physics of Fluids*, 36(3):031901, 2024.

[89] A. M. Smith and M. Stitt. Coordination of carbon supply and plant growth. *Plant, Cell & Environment*, 30(9):1126–1149, 2007.

[90] R. Stanfield, P. Schulte, K. Randolph, and U. Hacke. Computational models evaluating the impact of sieve plates and radial water exchange on phloem pressure gradients. *Plant, Cell & Environment*, 42(2):466–479, 2019.

[91] R. C. Stanfield, U. G. Hacke, and J. Laur. Are phloem sieve tubes leaky conduits supported by numerous aquaporins? *American Journal of Botany*, 104(5):719–732, 2017.

[92] S. Strogatz. *Nonlinear dynamics and chaos: with applications to physics, biology, chemistry, and engineering (studies in nonlinearity)*, volume 1. Westview press, 2001.

[93] R. Thaine. The protoplasmic-streaming theory of phloem transport. *Journal of Experimental Botany*, 15(3):470–484, 10 1964. ISSN 0022-0957. doi: 10.1093/jxb/15.3.470. URL https://doi.org/10.1093/jxb/15.3.470.

[94] R. Thom. Topological models in biology. *Topology*, 8(3):313–335, 1969.

[95] R. Thom. Structural stability, catastrophe theory, and applied mathematics. *SIAM review*, 19(2):189–201, 1977.

[96] R. Thom. *Structural stability and morphogenesis*. CRC press, 2018.

[97] M. Thompson and N. Holbrook. Application of a single-solute non-steady-state phloem model to the study of long-distance assimilate transport. *Journal of Theoretical Biology*, 220(4):419–455, 2003.

[98] M. Thompson and N. Holbrook. Scaling phloem transport: water potential equilibrium and osmoregulatory flow. *Plant, Cell & Environment*, 26(9):1561–1577, 2003.

[99] R. Thompson, H. Adams, D. Breshears, A. Collins, L. T. Dickman, C. Grossiord, A. Manrique-Alba, D. Peltier, M. Ryan, A. Trowbridge, et al. No carbon storage in growth-limited trees in a semi-arid woodland. *Nature Communications*, 14(1):1959, 2023.

[100] J. Thornley. A balanced quantitative model for root: shoot ratios in vegetative plants. *Annals of Botany*, 36(2):431–441, 1972.

[101] R. Turgeon. The puzzle of phloem pressure. *Plant Physiology*, 154(2):578–581, 2010.

[102] R. Turgeon. The role of phloem loading reconsidered. *Plant Physiology*, 152(4):1817–1823, 2010.

[103] M. Tyree. The cohesion-tension theory of sap ascent: current controversies. *Journal of Experimental Botany*, 48(10):1753–1765, 1997.

[104] A. van Bel. The phloem, a miracle of ingenuity. *Plant, Cell & Environment*, 26(1):125–149, 2003.

[105] T. Van den Honert. Water transport in plants as a catenary process. *Discussions of the Faraday Society*, 3:146–153, 1948.

[106] L. Vernon and S. Aronoff. Metabolism of soybean leaves. IV. translocation from soybean leaves. *Archives of Biochemistry and Biophysics*, 36(2):383–398, 1952.

[107] V. Volpe, S. Manzoni, M. Marani, and G. Katul. Leaf conductance and carbon gain under salt-stressed conditions. *Journal of Geophysical Research: Biogeosciences*, 116 (G4), 2011.

[108] A. Walker, A. Beckerman, L. Gu, J. Kattge, L. Cernusak, T. Domingues, J. Scales, G. Wohlfahrt, S. Wullschleger, and F. I. Woodward. The relationship of leaf photosynthetic traits–vcmax and jmax–to leaf nitrogen, leaf phosphorus, and specific leaf area: a meta-analysis and modeling study. *Ecology and Evolution*, 4(16):3218–3235, 2014.

[109] I. Wardlaw. Tansley Review No. 27: the control of carbon partitioning in plants. *New Phytologist*, 116(3):341–381, 1990.

[110] G. Weir. Analysis of Münch theory. *Mathematical Biosciences*, 56(1-2):141–152, 1981.

[111] D. R. Woodruff. The impacts of water stress on phloem transport in Douglas-fir trees. *Tree Physiology*, 34(1):5–14, 2014.

[112] E. Zeeman. Catastrophe theory. *Scientific American*, 234(4):65–83, 1976.